



Published in final edited form as:  
*Neuroimage*. 2007 October 15; 38(1): 34–42.

## A novel approach for imaging brain-behaviour relationships in mice reveals unexpected metabolic patterns during seizures in the absence of tissue plasminogen activator

Martine M. Mirrione<sup>1,2</sup>, Wynne K. Schiffer<sup>2</sup>, Joanna S. Fowler<sup>2</sup>, Dave L. Alexoff<sup>2</sup>, Stephen L. Dewey<sup>1,2,3</sup>, and Stella E. Tsirka<sup>1</sup>

<sup>1</sup>Graduate Program in Molecular and Cellular Pharmacology, State University of New York at Stony Brook, Stony Brook, New York 11794

<sup>2</sup>Medical Department, Brookhaven National Laboratory, Upton, New York 11973

<sup>3</sup>Psychiatry Department, New York University, School of Medicine, New York, New York 10016

### Abstract

Medically-refractory seizures cause inflammation and neurodegeneration. Seizure initiation thresholds have been linked in mice to the serine protease tissue plasminogen activator (tPA); mice lacking tPA exhibit resistance to seizure induction, and the ensuing inflammation and neurodegeneration are similarly suppressed. Seizure foci in humans can be examined using PET employing 2-deoxy-2-[<sup>18</sup>F]fluoro-D-glucose (<sup>18</sup>FDG) as a tracer to visualize metabolic dysfunction. However, there currently exist no such methods in mice to correlate measures of brain activation with behaviour. Using a novel method for small animal PET data analysis, we examine patterns of <sup>18</sup>FDG uptake in wild type and tPA<sup>-/-</sup> mice and find that they correlate with the severity of drug-induced seizure initiation. Furthermore, we report unexpected activations that may underlie the tPA modulation of seizure susceptibility. The methods described here should be applicable to other mouse models of human neurological disease.

### INTRODUCTION

Increased hippocampal excitability is commonly observed in temporal lobe epilepsy (TLE) (Carne et al., 2004; de Lanerolle et al., 2003) and can be visualized indirectly using metabolic imaging of 2-deoxy-2-[<sup>18</sup>F]fluoro-D-glucose (<sup>18</sup>FDG) (Diehl et al., 2003; Lamusuo et al., 2001). Small animal imaging using microPET has become an increasingly useful tool in multiple research areas (Schiffer et al., 2005; Schiffer et al., 2006a; Sossi and Ruth, 2005). However, existing image analysis strategies for small animal PET data are targeted toward examining regional changes in <sup>18</sup>FDG uptake, as we have shown for an animal model of TLE (Mirrione et al., 2006). Here we describe a way to use statistical parametric mapping (SPM), an advanced image analysis strategy commonly used in human imaging studies, to develop a high-throughput and clinically relevant method to elucidate brain/behaviour relationships in animal models of human disease.

Manuscript correspondence should be addressed to Stella E. Tsirka; Tel: 6314443859; Email: stella@pharm.stonybrook.edu. Correspondence and requests for materials should be addressed to W.K.S (wynne@bnl.gov).

The authors declare no competing financial interests.

**Publisher's Disclaimer:** This is a PDF file of an unedited manuscript that has been accepted for publication. As a service to our customers we are providing this early version of the manuscript. The manuscript will undergo copyediting, typesetting, and review of the resulting proof before it is published in its final citable form. Please note that during the production process errors may be discovered which could affect the content, and all legal disclaimers that apply to the journal pertain.

We have previously reported that mice deficient in tissue plasminogen activator (tPA<sup>-/-</sup>) display a higher threshold for seizure onset using an animal model for TLE (Tsirka et al., 1995). tPA is expressed in the central nervous system (CNS) and plays a role in neuronal plasticity (Baranes et al., 1998; Centonze et al., 2002; Madani et al., 1999; Seeds et al., 1995; Zhuo et al., 2000) and seizure susceptibility (Pawlak et al., 2005; Qian et al., 1993; Tsirka et al., 1995; Yepes et al., 2002). In metrazol (PTZ)-induced seizures and kindling, tPA is transcriptionally up-regulated in pyramidal neurons of the hippocampus and thought to contribute to structural changes observed following activity dependent plasticity (Carroll et al., 1994; Qian et al., 1993). The changes include physiological elongation of mossy fiber axons during late-phase long-term potentiation (LTP) (Baranes et al., 1998; Madani et al., 1999; Zhuo et al., 2000) and aberrant neurite outgrowth (Salles and Strickland, 2002; Wu et al., 2000; Zhang et al., 2005). We have developed a unique method to test the relationship between seizure severity and brain activation, and have specifically examined whether tPA<sup>-/-</sup> mice demonstrate an altered pattern of metabolic activation.

At the core of the method is the necessity for small animal image analysis strategies to keep up with the rapidly expanding role of imaging in animal models of human disease. Small animal MRI, PET and CT systems are now commercially available, and there is a commensurate need for image analysis strategies to take full advantage of these preclinical imaging systems. We describe a high-throughput approach for neurological mouse small animal PET data analysis that includes streamlined spatial pre-processing of imaging data in atlas space and implementation of a voxel-based correlation analysis widely used to elucidate brain-behaviour relationships in human functional brain imaging. The voxel-based analysis has been validated using a traditional ROI analysis coupled to behavioural scores with a linear approach we previously described (Mirrione et al., 2006). Our results suggest that the relationships observed between metabolic activity and seizure severity in wild type mice do not hold in tPA<sup>-/-</sup> mice. These results provide *in vivo* evidence of a discord between brain activity and behaviour in the genetically modified animals. The integrated approach to experimental design and data analysis can be applied to a broad spectrum of research involving genetically altered mice. We describe tools, including a whole brain mouse ROI template in stereotaxic space (Paxinos and Franklin, 2001), implementation of methods for voxel-based analysis of mouse brain function using the SPM software package, and high throughput procedures for experimental design using serial studies.

## MATERIALS AND METHODS

### Mouse seizure model

Animal procedures were approved by the Institute for Animal Care and Use Committee (IACUC) at Stony Brook and Brookhaven National Laboratory (BNL). Mice, aged 2-5 months, 24-34 grams, were obtained from either Taconic farms or transferred to BNL from Stony Brook University DLAR. All animals received two PET scans, 7 days apart. For the first (baseline) scan each animal underwent 45 min of <sup>18</sup>F<sup>18</sup>FDG uptake followed by 100mg/kg of a 10% xylazine, 90% ketamine anaesthesia for a 10-min scan. Seizure severity was scored on a scale of 0-6; 0: normal behavior; 1: immobility; 2: forelimb and/or tail extension, rigid posture; 3: repetitive movements, head bobbing; partial body clonus 4: rearing; 5: continuous rearing and falling, whole body clonus; 6: severe tonic-clonic seizures with loss of posture or jumping (Racine et al., 1972; Schauwecker and Steward, 1997). To ensure objectivity, scores were assigned when symptoms in that category were observed at least three times. Whole blood glucose was subsequently measured using a glucometer (CVS brand). For the second scan, seizures were induced using pilocarpine (Sigma) (280mg/kg, i.p.) (Mirrione et al., 2006; Schauwecker and Steward, 1997). Methyl-scopolamine (Sigma) pre-treatment (2mg/kg) 15-30 min prior,

reduces peripheral cholinergic effects of pilocarpine, and by itself does not alter  $^{18}\text{F}$ FDG (Supplementary Figure 3).

### MicroPET data acquisition

Metabolic imaging was performed using a microPET R4 tomograph (Concorde Microsystems, Knoxville, TN) with a transaxial resolution of 1.8mm full width at half maximum (FWHM) using methods previously reported (Mirrione et al., 2006). MicroPET sinograms were corrected for photon scatter (Alexoff et al., 2003), and were reconstructed using the maximum likelihood expectation maximization (MLEM) algorithm with 20 iterations and a pixel size of  $0.4 \times 0.4 \times 1.2$  mm (Schiffer et al., 2006b).

### Spatial Preprocessing & Templates

The MRI reference template (Ma et al., 2005) was given a voxel size of  $2 \times 2 \times 2$  mm. The bounding box (a 3-dimensional space that defines the template space) encompassed the following x, y, z dimensions and origin in mm (-82, 82; -130, 130; -102, 26), (82, 130, 102). A volumetric ROI template was created based on the segmented MRI dataset (Ma et al., 2005) using PMOD contour tool (<http://www.pmod.com>). All MLEM reconstructed  $\mu\text{PET}$  images (n=50) were matched to the MRI template using PMOD Fusion Toolbox. This software package automatically adjusts the voxel spacing, origin, and dimensions of the bounding box to match the atlas.

Spatial normalization is more accurate if the target radioactivity distribution, or template, is similar to each individual scan (Gispert et al., 2003). Since the difference in regional  $^{18}\text{F}$ FDG uptake between the baseline and experimental conditions was high (e.g. during seizures there was much more FDG uptake in the hippocampus relative to the cortex or surrounding tissue), condition-specific templates were generated (Supplementary Fig.1). To make the  $^{18}\text{F}$ FDG templates, all baseline (n=25) or treatment (n=25) images, regardless of genotype, were coregistered to a respective image using SPM2, (<http://www.fil.ion.ucl.ac.uk/spm>). Parameters included normalized mutual information cost function and trilinear reslicing. The resulting individual images were averaged to make two mean images (baseline and pilocarpine treated). These were aligned to each other and with the MRI reference template. The normal (baseline) template was coregistered to the MRI atlas first and used to align the treatment-specific template using both automated and manual registration. Both templates were spatially smoothed with an isotropic Gaussian kernel (6 mm FWHM) to remove any subtle non-uniformities. Individual images were realigned and coregistered using the respective  $^{18}\text{F}$ FDG templates. Parameters for realignment included trilinear reslice interpolation. Normalization employed affine transformations with trilinear interpolation and preserved concentrations.

### Data Analysis

The ROI template was overlaid on individual normalized image datasets and statistics were calculated based on mean pixel value in each ROI using PMOD software. Average radiotracer concentration in each region was normalized to the average value in the whole brain using the following equation (1):

$$\text{ROI : whole brain} = \frac{\text{ROI value}}{\text{Whole Brain value}} \quad (1)$$

Individual images were globally normalized using the image algebra function in PMOD where image pixel was divided by the mean pixel value in the image. This yields a parametric image for each scan on an identical scale. As part of the analysis, individual images were then averaged to create mean images representative of changes in  $^{18}\text{F}$ FDG uptake within each group.

Voxel-based statistical analyses were done with SPM. The analysis design selected was ‘PET multi-subject condition and covariate’ for the comparisons of baseline and pilocarpine-treatment, where baseline was entered as (0) the first condition, and pilocarpine-treatment was entered as (1) the second condition. Seizure scores (determined on a scale of 1 to 6) were converted into a covariate centered on the baseline score of 0, therefore were entered -3 to 3. To model the main effect of a seizure, the contrast was set at -1, 1, 0 for increases in  $^{18}\text{F}$  uptake resulting from pilocarpine treatment. To model the parametric effect of seizure severity, the contrast was set at 0, 0, 1, (centered around the overall mean) providing the behavioral correlation. Model parameters included global normalization, where proportional scaling was set at 100 and absolute threshold masking at 0.05. The mean voxel value was calculated (within per image full mean /8 mask). Non-sphericity correction was used with replications over subjects and correlated repeated measures were defined. Parameters were estimated and contrast images were computed using the  $t$  statistic, which generated statistical parametric maps of  $t$ -values. The  $t$  contrasts were defined as pilocarpine-treatment minus baseline for regions that increased during seizures, and baseline minus pilocarpine-treatment for regions that decreased. The statistical threshold ( $t$  or  $p$  value) was set at  $p < 0.05$ ,  $p < 0.01$ , or  $p < 0.001$  (non-sphericity corrected) with an extent threshold of 100 contiguous voxels.  $T$ -value maps of seizures were overlaid on coronal and transverse views of the MRI reference template to define the voxels with significant change.

### Statistical Analyses

All additional statistics were performed using GraphPad Prism 4.00 for Windows, GraphPad Software (<http://www.graphpad.com>) or Microsoft Excel. Data from seizure scoring were analyzed by Student’s  $t$ -test. Parameter measures (glucose, weight, dose, and uptake) were analyzed by one-way ANOVA with *group* as a factor, and Barlett’s test to verify equal variances. ROI data were analyzed using two-way ANOVA for repeated measurements with *treatment* as a factor, and Bonferroni post-tests to determine significance levels among ROIs. Significance level of correlation plots was determined by Pearson Coefficient & Regression Analysis. All data were normally distributed.

## RESULTS

### Region of Interest (ROI) Template

The C57Bl/6J (wt) mouse whole brain *ex vivo* MRI reference template (Ma et al., 2005) was employed for mapping regional changes in  $^{18}\text{F}$  uptake. This atlas was placed in stereotaxic space (Paxinos and Franklin, 2001) using established methods (Schweinhart et al., 2003) where several known points spread uniformly around the brain were used to validate its placement. A volumetric ROI template was created based on 20 regions segmented from the MRI template (Ma et al., 2005). In Fig. 1a, this template was overlaid on the atlas. All ROI volumes were within the resolution of maximum likelihood-expectation maximization (MLEM) reconstructed microPET data (5 mm<sup>3</sup> or ~5 $\mu\text{l}$  (Abbey et al., 2004) at the center of the field of view and based on a 10nsec timing window). The center coordinates and volumes for each region are reported in Table 1. Image fitting to this ROI template required that each condition be normalized to a unique template (Supplementary Fig1).

### Validation of Longitudinal Design

The longitudinal design in this study (two PET scans, baseline and experimental, separated by 7 days) was validated for both genotypes (wt  $n=4$ , tPA<sup>-/-</sup>  $n=3$ ). Correlations between structures over whole brain ROI values were calculated by plotting the average  $^{18}\text{F}$  uptake in ROIs for scan 1 over scan 2 (Fig. 1g,h). A significant correlation was observed (wt,  $r^2=0.94$ , slope= $1.15 \pm 0.04$ ,  $p < 0.0001$ ; tPA<sup>-/-</sup>,  $r^2=0.88$ , slope= $0.83 \pm 0.049$ ,  $p < 0.0001$ ). Percent differences between average ROIs were calculated as means for determining reliability

(Supplementary Fig.2). The values in most regions were within  $\pm 5\%$  between the two scans, while in smaller regions (hypothalamus and amygdala) values were  $> \pm 10\%$  (see Table 1 for ROI volume). On average, all relevant ROIs were within an acceptably reproducible range.

### Neuronal activity during seizures

On the scan day, a pre-treatment of methyl scopolamine was given to reduce peripheral cholinergic effects. Methyl scopolamine alone did not alter  $^{18}\text{F}$ FDG uptake (Supplementary Fig. 3). Administration of pilocarpine was used to induce seizures. After the pilocarpine injection, animals were injected with  $^{18}\text{F}$ FDG and videotaped during radiotracer uptake. Only mice that survived the entire radiotracer uptake period are reported here (survival rates given below).

We determined the seizure score in wt and tPA<sup>-/-</sup> animals (Fig.2c). In the wt group, 42.9% (6/14) of mice experienced stage 4-6 level seizures, while the tPA<sup>-/-</sup> animals showed attenuated symptoms (none were categorized above stage 3). Three tPA<sup>-/-</sup> animals did have a single isolated stage 4-6 level seizure, which did not generalize. There was a significant correlation between behaviour and hippocampal  $^{18}\text{F}$ FDG uptake in wt ( $r=0.59$ ,  $p=0.03$ ,  $r^2=0.35$ ; Fig.2d), but not tPA<sup>-/-</sup> animals ( $r=0.42$ ,  $p=0.18$ ,  $r^2=0.22$ ; Fig.2e). However, differences were noted in survival rate of the genotypes. An overall higher mortality rate was observed in tPA<sup>-/-</sup> mice, as 50% pilocarpine-injected died from seizures during uptake (11/22), compared to only 21% (3/14) wt mice, as reported (Shibley and Smith, 2002).

### ROI analysis results

Individual images were skull stripped to remove extra-cranial signal, and pixel values were normalized by dividing the image by the average whole brain pixel value. In each group, normalized datasets were averaged to create mean images of radioactivity distributions (Fig 2a). In the transverse plane, arrows designate enhanced regional  $^{18}\text{F}$ FDG uptake in tPA<sup>-/-</sup> mice compared to wt. The ROI template was overlaid on individual images after spatial pre-processing (coregistration & normalization) and the average radioactivity concentration within each ROI and the whole brain was determined. Regional changes in  $^{18}\text{F}$ FDG uptake compared to the whole brain were calculated using Equation 1. The percent difference between baseline and pilocarpine-treatment was determined for each pair of scans (Fig.2b). There was a significant main effect for region ( $F_{112}=35.13$ ,  $p<0.001$ ), where pilocarpine-treatment significantly increased FDG uptake in the hippocampus (HIP), and thalamus (THA). tPA<sup>-/-</sup> mice showed significant activations in the midbrain (MID) and cerebellum (CB), HIP, superior and inferior colliculi (SC and IC, respectively).  $^{18}\text{F}$ FDG uptake was significantly different between genotypes in the olfactory bulb (OLF,  $p = 0.009$ ), where wt mice showed less activation in this region than tPA<sup>-/-</sup> animals. Both genotypes displayed pilocarpine-induced decreases in the cortex (CTX), basal forebrain/septum (BFS), amygdala (AMY), and brain stem (BS).

### SPM method results

A voxel-based analysis was performed using SPM2 (<http://www.fil.ion.ucl.ac.uk/spm>) on normalized images, where individual serial scans were compared at baseline and pilocarpine-treatment (wt  $n=14$  and tPA<sup>-/-</sup>  $n=11$ ). This analysis takes into account repeated measures of the paired study and reveals significant changes between conditions among the scan pairs. SPM results revealed unique patterns in  $^{18}\text{F}$ FDG uptake dependent on genotype. Activations are presented as areas of increased  $^{18}\text{F}$ FDG uptake from baseline to pilocarpine-treatment (Fig.3). There were clusters of activation present in HIP, BFS (dashed arrow, Fig.3a), and THA (arrow, Fig.3a;  $p<0.001$  corrected) which appear more widespread in wt than tPA<sup>-/-</sup> mice. The activations were consistent with behavioural data, as wt mice experienced greater seizure severity compared to tPA<sup>-/-</sup> animals (Fig.2g). In agreement with the ROI analysis, regions such as the OLF were less activated in the wt compared to tPA<sup>-/-</sup> animals.

Finally, SPM provides the unique opportunity to search all of the voxels in all of the brains and identify those voxels which vary together with behaviour. When this covariate analysis was performed, different clusters of voxels increased with seizure severity depending on the genotype of the animal (Fig.3c,f). For example, the relationship between hippocampal activation and seizure severity encompassed most of the ventral hippocampus in wt animals, but not in tPA<sup>-/-</sup> animals.

### Additional factors

Additional parameters that could influence <sup>18</sup>FDG uptake in animals included blood glucose levels, radiotracer dose, weight of the animal, and exact uptake time, although the ratio method used here to compare the data would cancel out effects caused by such variability. The distribution of these parameters within treatments was determined, and statistical analysis showed that the ROI values from each group were normally distributed and not significantly different from each other (one-way ANOVA, *parameters, genotype and treatment*; see mean  $\pm$ SEM in Table 1).

## DISCUSSION

In this study we developed and validated a novel strategy for small animal PET data analysis, and present a novel way to correlate brain activity and behaviour. We compare changes in mouse brain <sup>18</sup>FDG uptake between baseline conditions and seizures. To our knowledge, this is the first study to streamline whole brain analysis methods using an in-house ROI template with voxel-wise correlations of brain activity and behaviour in genetically modified mice. Using voxel-based SPM2, we show that tPA<sup>-/-</sup> mice exhibit unique patterns of metabolic activation compared to wt animals.

### tPA modulates seizure threshold

A modulatory role for tPA in synaptic plasticity and neuronal activation during seizures has been reported and existing methods have shown both changes in brain activity (Baranes et al., 1998) and changes in seizure severity (Pawlak et al., 2005; Tsirka et al., 1995), but there was no method to correlate these isolated findings in the same model. In fact, our previous data showed that deficiency in tPA results in a higher threshold for pharmacologically-induced epilepsy (Tsirka et al., 1995). We thus hypothesized that reduced seizure severity observed in the absence of tPA would correlate with decreased neuronal activity measured by <sup>18</sup>FDG. To test this hypothesis, we devised a new method to explore these relationships in the same animal. Using this approach, we found that seizure symptoms were weaker in tPA<sup>-/-</sup> mice and some regions showed specific attenuation in <sup>18</sup>FDG uptake (hippocampus, septum and thalamus, Fig.3). In addition to regionally-specific attenuation of <sup>18</sup>FDG uptake, SPM analysis revealed that tPA<sup>-/-</sup> mice show increased activation in the cerebellum, olfactory bulb and areas of the midbrain including the inferior and superior colliculi (Fig.3). Additional cerebellar activations seen in the tPA<sup>-/-</sup> mice may be due to sudden inhibitions of motor control, previously attributed to increases in amino acid release in the cerebellum (Smolders et al., 1997).

Pilocarpine-treated mice show alterations in electroencephalograms starting in the hippocampus and spreading to cortical regions (Turski et al., 1984). Our data reveal increased <sup>18</sup>FDG uptake in the hippocampus during early, acute seizures (Fig.2, 3). Other reports show similar regional changes in <sup>18</sup>FDG uptake in seizure rodent models (Kornblum et al., 2000). Pilocarpine preferentially binds muscarinic (M1) acetylcholine receptors (Hamilton et al., 1997) which are required for the initiation, but not maintenance, of seizures (Maslanski et al., 1994). M1 receptors are expressed in the cortex, thalamus, hippocampus and septum and their stimulation may initiate seizures that recruit noncholinergic systems, specifically NMDARs. tPA induces proteolytic cleavage of the NR1 subunit of the NMDAR

which is thought to enhance NMDAR signalling (Nicole et al., 2001). This may contribute to differences observed in  $tPA^{-/-}$  mice in seizure behaviour and specific regional  $^{18}F$ FDG uptake, despite robust hippocampal activation above baselines.  $^{18}F$ FDG could reveal increases in firing rates caused by M1 stimulation; seizures, however, may not propagate beyond the hippocampus because of reduced ability to activate NMDARs, which would result in behavioural differences between the genotypes.

A significant positive correlation was observed between hippocampal  $^{18}F$ FDG uptake and seizure score in wild-type mice, which did not seem to hold true in  $tPA^{-/-}$  mice. This lack of correlation in  $tPA^{-/-}$  animals may reflect deficiencies in hippocampal circuitry in the mutant mice, as evident in other examples of hippocampal activity [i.e., deficiency in late phase LTP (Frey et al., 1996; Baranes et al., 1998)], or defects in seizure spreading.

Although the septum is smaller than the resolution of microPET, SPM analysis showed higher  $^{18}F$ FDG uptake in wt mice correlated with seizure activity (Fig.3). Septal GABAergic neurons project to the hippocampus and are particularly vulnerable to degeneration during pilocarpine-induced seizures (Garrido Sanabria et al., 2006). These inhibitory neurons normally undergo excitotoxic death during the acute seizure induction phase (perhaps resulting in increased  $^{18}F$ FDG uptake), and thus have the potential to modulate seizure spread differentially in the two genotypes. However, there was a discrepancy between ROI basal forebrain and septum and SPM results. This may have been avoided, if this particular ROI could be further subdivided.

Potentiated GABAergic transmission in the hippocampal CA1 region of  $tPA^{-/-}$  mice (Frey et al., 1996) may be a signature of an overall reduced baseline excitatory drive in these mice. Future studies may determine potential abnormalities in neurotransmitter release in  $tPA^{-/-}$  mice during seizures. Monitoring extracellular glutamate, aspartate and GABA concentrations in the hippocampus after local pilocarpine infusion shows that these neurotransmitters play a role in seizure maintenance and/or spread, not necessarily onset (Smolders et al., 1997). It is possible that  $tPA^{-/-}$  mice have alterations in stimulation-induced neurotransmitter release. The data presented here suggest lack of seizure spreading mechanisms instead of reduced excitatory potential in the absence of tPA.

## Limitations of this study

During limbic seizures and the interictal period, changes in metabolic activity and cerebral blood flow occur (Pereira de Vasconcelos et al., 2002; Tanaka et al., 1990). Therefore, differences in neuronal activations may reflect this, although  $^{18}F$ FDG is generally considered more sensitive to glucose transporter occupancy and blood glucose changes than blood flow itself (Schmidt et al., 1996). Our datasets were normalized to remove the effects of blood flow by using ratios, not by addressing any absolute changes in  $^{18}F$ FDG uptake between groups (or metabolic rates of glucose).

Normalizing images by calculating the ROI to whole brain ratio reveals regional changes in activity. This method is robust as it reduces inter-subject variability, however is limited, as differences between groups in the absolute level of metabolic activation would be obscured (Signorini et al., 1999). Nevertheless, pilocarpine treatment results in regional changes that are prominent (Scorza et al., 2002). It is possible that brain  $^{18}F$ FDG uptake is increased from seizures to a different extent in the two genotypes which cannot be detected by normalizing each ROI value to the mean pixel value. Lower starting glucose levels in  $tPA^{-/-}$  mice could confound results, since less endogenous competition for glucose transporters would increase  $^{18}F$ FDG uptake.

There is increased demand for developing methods to analyze small animal PET data. Iterative reconstruction algorithms, such as MLEM, are now routinely employed to increase resolution to determine quantitative regional differences in the brain (Nuyts and Fessler, 2003). However, inherent technical limitations (resolution and partial volume effects) become challenging when studies involve neurological imaging in mice. Iterative reconstruction somewhat corrects for partial volume effects but there remains some underestimation of activity concentrations in regions below the resolution of the MLEM reconstructed data. Additionally, facial glands (salivary, lacrimal and harderian) produce “spill-over” effects, even after iterative reconstruction. While the improved resolution by iterative reconstruction allows for more refined analysis, results from small brain regions ( $\leq 5 \text{ mm}^3$ ) or those susceptible to spill-over effects need to be interpreted with caution. All the ROIs reported here are  $> 5 \text{ mm}^3$ . However some regions, e.g. the inferior and superior colliculi, are subject to spill-over effects from the hippocampus, especially when hippocampal  $^{18}\text{F}$ FDG uptake is high (pilocarpine-treated group).

## Conclusions

Here we demonstrate the successful use of  $^{18}\text{F}$ FDG as a marker for metabolic changes associated with seizure activity. We have demonstrated the potential for correlating behaviour and disease symptoms with brain function *in-vivo*. Our data show the relationship between metabolic activity and behaviour is not sustained in  $t\text{PA}^{-/-}$  animals suggesting these animals have an altered response to seizure induction. Furthermore, the methods validated here for small animal PET data analysis can be applied to other areas of research in other mouse models of disease.

## Supplementary Material

Refer to Web version on PubMed Central for supplementary material.

## Acknowledgements

The authors would like to thank members of the BNL cyclotron facility, Michael Schueller, David J. Schyler, Colleen Shea, and Youwen Xu, for  $^{18}\text{F}$ FDG preparation. We would also like to thank Shiva Kothari for assistance in verifying baseline glucose levels between genotypes. This work was supported by National Institutes of Health (R01NS42168) and American Heart Association-Established Investigator Award (S.E.T) and USDOE/OBER DE-AC02-98CH10886 and NIDA DA15041 and DA15082 (S.L.D).

## References

- Abbey CK, Borowsky AD, McGoldrick ET, Gregg JP, Maglione JE, Cardiff RD, Cherry SR. In vivo positron-emission tomography imaging of progression and transformation in a mouse model of mammary neoplasia. *Proc Natl Acad Sci U S A* 2004;101:11438–11443. [PubMed: 15277673]
- Alexoff DL, Vaska P, Marsteller D, Gerasimov T, Li J, Logan J, Fowler JS, Taintor NB, Thanos PK, Volkow ND. Reproducibility of  $^{11}\text{C}$ -raclopride binding in the rat brain measured with the microPET R4: effects of scatter correction and tracer specific activity. *J Nucl Med* 2003;44:815–822. [PubMed: 12732684]
- Baranes D, Lederfein D, Huang YY, Chen M, Bailey CH, Kandel ER. Tissue plasminogen activator contributes to the late phase of LTP and to synaptic growth in the hippocampal mossy fiber pathway. *Neuron* 1998;21:813–825. [PubMed: 9808467]
- Carne RP, O'Brien TJ, Kilpatrick CJ, MacGregor LR, Hicks RJ, Murphy MA, Bowden SC, Kaye AH, Cook MJ. MRI-negative PET-positive temporal lobe epilepsy: a distinct surgically remediable syndrome. *Brain* 2004;127:2276–2285. [PubMed: 15282217]
- Carroll PM, Tsirka SE, Richards WG, Frohman MA, Strickland S. The mouse tissue plasminogen activator gene 5' flanking region directs appropriate expression in development and a seizure-enhanced response in the CNS. *Development* 1994;120:3173–3183. [PubMed: 7720560]

- Centonze D, Napolitano M, Saulle E, Gubellini P, Picconi B, Martorana A, Pisani A, Gulino A, Bernardi G, Calabresi P. Tissue plasminogen activator is required for corticostriatal long-term potentiation. *Eur J Neurosci* 2002;16:713–721. [PubMed: 12270047]
- de Lanerolle NC, Kim JH, Williamson A, Spencer SS, Zaveri HP, Eid T, Spencer DD. A retrospective analysis of hippocampal pathology in human temporal lobe epilepsy: evidence for distinctive patient subcategories. *Epilepsia* 2003;44:677–687. [PubMed: 12752467]
- Diehl B, LaPresto E, Najm I, Raja S, Rona S, Babb T, Ying Z, Bingaman W, Luders HO, Ruggieri P. Neocortical temporal FDG-PET hypometabolism correlates with temporal lobe atrophy in hippocampal sclerosis associated with microscopic cortical dysplasia. *Epilepsia* 2003;44:559–564. [PubMed: 12681005]
- Frey U, Müller M, Kuhl D. A different form of long-lasting potentiation revealed in tissue plasminogen activator mutant mice. *J Neurosci* 1996;16:2057–2063. [PubMed: 8604050]
- Garrido Sanabria ER, Castaneda MT, Banuelos C, Perez-Cordova MG, Hernandez S, Colom LV. Septal gabaergic neurons are selectively vulnerable to pilocarpine-induced status epilepticus and chronic spontaneous seizures. *Neuroscience*. 2006
- Gispert JD, Pascau J, Reig S, Martinez-Lazaro R, Molina V, Garcia-Barreno P, Desco M. Influence of the normalization template on the outcome of statistical parametric mapping of PET scans. *Neuroimage* 2003;19:601–612. [PubMed: 12880791]
- Hamilton SE, Loose MD, Qi M, Levey AI, Hille B, McKnight GS, Idzerda RL, Nathanson NM. Disruption of the m1 receptor gene ablates muscarinic receptor-dependent M current regulation and seizure activity in mice. *Proc Natl Acad Sci U S A* 1997;94:13311–13316. [PubMed: 9371842]
- Kornblum HI, Araujo DM, Annala AJ, Tatsukawa KJ, Phelps ME, Cherry SR. In vivo imaging of neuronal activation and plasticity in the rat brain by high resolution positron emission tomography (microPET). *Nat Biotechnol* 2000;18:655–660. [PubMed: 10835605]
- Lamusuo S, Jutila L, Ylinen A, Kalviainen R, Mervaala E, Haaparanta M, Jaaskelainen S, Partanen K, Vapalahti M, Rinne J. [18F]FDG-PET reveals temporal hypometabolism in patients with temporal lobe epilepsy even when quantitative MRI and histopathological analysis show only mild hippocampal damage. *Arch Neurol* 2001;58:933–939. [PubMed: 11405808]
- Ma Y, Hof PR, Grant SC, Blackband SJ, Bennett R, Slatest L, McGuigan MD, Benveniste H. A three-dimensional digital atlas database of the adult C57BL/6J mouse brain by magnetic resonance microscopy. *Neuroscience* 2005;135:1203–1215. [PubMed: 16165303]
- Madani R, Hulo S, Toni N, Madani H, Steimer T, Muller D, Vassalli JD. Enhanced hippocampal long-term potentiation and learning by increased neuronal expression of tissue-type plasminogen activator in transgenic mice. *Embo J* 1999;18:3007–3012. [PubMed: 10357813]
- Maslanski JA, Powelt R, Deirmengiant C, Patel J. Assessment of the muscarinic receptor subtypes involved in pilocarpine-induced seizures in mice. *Neurosci Lett* 1994;168:225–228. [PubMed: 8028781]
- Mirrione MM, Schiffer WK, Siddiq M, Dewey SL, Tsirka SE. PET imaging of glucose metabolism in a mouse model of temporal lobe epilepsy. *Synapse* 2006;59:119–121. [PubMed: 16320304]
- Nicole O, Docagne F, Ali C, Margail I, Carmeliet P, MacKenzie ET, Vivien D, Buisson A. The proteolytic activity of tissue-plasminogen activator enhances NMDA receptor-mediated signaling. *Nat Med* 2001;7:59–64. [PubMed: 11135617]
- Nuyts J, Fessler JA. A penalized-likelihood image reconstruction method for emission tomography, compared to postsmoothed maximum-likelihood with matched spatial resolution. *IEEE Trans Med Imaging* 2003;22:1042–1052. [PubMed: 12956260]
- Pawlak R, Melchor JP, Matys T, Skrzypiec AE, Strickland S. Ethanol-withdrawal seizures are controlled by tissue plasminogen activator via modulation of NR2B-containing NMDA receptors. *Proc Natl Acad Sci U S A* 2005;102:443–448. [PubMed: 15630096]
- Paxinos, G.; Franklin, KBJ. *The mouse brain in stereotaxic coordinates*. 2. Academic Press; San Diego: 2001.
- Pereira de Vasconcelos A, Ferrandon A, Nehlig A. Local cerebral blood flow during lithium-pilocarpine seizures in the developing and adult rat: role of coupling between blood flow and metabolism in the genesis of neuronal damage. *J Cereb Blood Flow Metab* 2002;22:196–205. [PubMed: 11823717]

- Qian Z, Gilbert ME, Colicos MA, Kandel ER, Kuhl D. Tissue-plasminogen activator is induced as an immediate-early gene during seizure, kindling and long-term potentiation. *Nature* 1993;361:453–457. [PubMed: 8429885]
- Racine R, Gartner J, Burnham W. Epileptiform activity and neural plasticity in limbic structures. *Brain Res* 1972;47:262–268. [PubMed: 4641271]
- Salles FJ, Strickland S. Localization and regulation of the tissue plasminogen activator-plasmin system in the hippocampus. *J Neurosci* 2002;22:2125–2134. [PubMed: 11896152]
- Schauwecker PE, Steward O. Genetic determinants of susceptibility to excitotoxic cell death: implications for gene targeting approaches. *Proc Natl Acad Sci U S A* 1997;94:4103–4108. [PubMed: 9108112]
- Schiffer WK, Alexoff DL, Shea C, Logan J, Dewey SL. Development of a simultaneous PET/microdialysis method to identify the optimal dose of 11C-raclopride for small animal imaging. *J Neurosci Methods* 2005;144:25–34. [PubMed: 15848236]
- Schiffer WK, Lee DE, Alexoff DL, Ferrieri R, Brodie JD, Dewey SL. Metabolic correlates of toluene abuse: decline and recovery of function in adolescent animals. *Psychopharmacology (Berl)* 2006a;186:159–167. [PubMed: 16703400]
- Schiffer WK, Mirrione MM, Biegen A, Alexoff DL, Patel V, Dewey SL. Serial microPET measures of the metabolic reaction to a microdialysis probe implant. *J Neurosci Methods*. 2006b
- Schmidt KC, Lucignani G, Sokoloff L. Fluorine-18-fluorodeoxyglucose PET to determine regional cerebral glucose utilization: a re-examination. *J Nucl Med* 1996;37:394–399. [PubMed: 8667082]
- Schweinhardt P, Fransson P, Olson L, Spenger C, Andersson JL. A template for spatial normalisation of MR images of the rat brain. *J Neurosci Methods* 2003;129:105–113. [PubMed: 14511814]
- Scorza FA, Arida RM, Priel MR, Calderazzo L, Cavalheiro EA. Glucose utilisation during status epilepticus in an epilepsy model induced by pilocarpine: a qualitative study. *Arq Neuropsiquiatr* 2002;60:198–203. [PubMed: 12068345]
- Seeds NW, Williams BL, Bickford PC. Tissue plasminogen activator induction in Purkinje neurons after cerebellar motor learning. *Science* 1995;270:1992–1994. [PubMed: 8533091]
- Shibley H, Smith BN. Pilocarpine-induced status epilepticus results in mossy fiber sprouting and spontaneous seizures in C57BL/6 and CD-1 mice. *Epilepsy Res* 2002;49:109–120. [PubMed: 12049799]
- Signorini M, Paulesu E, Friston K, Perani D, Colleluori A, Lucignani G, Grassi F, Bettinardi V, Frackowiak RS, Fazio F. Rapid assessment of regional cerebral metabolic abnormalities in single subjects with quantitative and nonquantitative [<sup>18</sup>F]FDG PET: A clinical validation of statistical parametric mapping. *Neuroimage* 1999;9:63–80. [PubMed: 9918728]
- Smolders I, Van Belle K, Ebinger G, Michotte Y. Hippocampal and cerebellar extracellular amino acids during pilocarpine-induced seizures in freely moving rats. *Eur J Pharmacol* 1997;319:21–29. [PubMed: 9030893]
- Sossi V, Ruth TJ. MicroPET imaging: in vivo biochemistry in small animals. *J Neural Transm* 2005;112:319–330. [PubMed: 15723157]
- Tanaka S, Sako K, Tanaka T, Nishihara I, Yonemasu Y. Uncoupling of local blood flow and metabolism in the hippocampal CA3 in kainic acid-induced limbic seizure status. *Neuroscience* 1990;36:339–348. [PubMed: 2120614]
- Tsirka SE, Gualandris A, Amaral DG, Strickland S. Excitotoxin-induced neuronal degeneration and seizure are mediated by tissue plasminogen activator. *Nature* 1995;377:340–344. [PubMed: 7566088]
- Turski WA, Cavalheiro EA, Bortolotto ZA, Mello LM, Schwarz M, Turski L. Seizures produced by pilocarpine in mice: a behavioral, electroencephalographic and morphological analysis. *Brain Res* 1984;321:237–253. [PubMed: 6498517]
- Wu YP, Siao CJ, Lu W, Sung TC, Frohman MA, Milev P, Bugge TH, Degen JL, Levine JM, Margolis RU, Tsirka SE. The tissue plasminogen activator (tPA)/plasmin extracellular proteolytic system regulates seizure-induced hippocampal mossy fiber outgrowth through a proteoglycan substrate. *J Cell Biol* 2000;148:1295–1304. [PubMed: 10725341]
- Yepes M, Sandkvist M, Coleman TA, Moore E, Wu JY, Mitola D, Bugge TH, Lawrence DA. Regulation of seizure spreading by neuroserpin and tissue-type plasminogen activator is plasminogen-independent. *J Clin Invest* 2002;109:1571–1578. [PubMed: 12070304]

- Zhang Y, Kanaho Y, Frohman MA, Tsirka SE. Phospholipase D1-promoted release of tissue plasminogen activator facilitates neurite outgrowth. *J Neurosci* 2005;25:1797–1805. [PubMed: 15716416]
- Zhuo M, Holtzman DM, Li Y, Osaka H, DeMaro J, Jacquin M, Bu G. Role of tissue plasminogen activator receptor LRP in hippocampal long-term potentiation. *J Neurosci* 2000;20:542–549. [PubMed: 10632583]

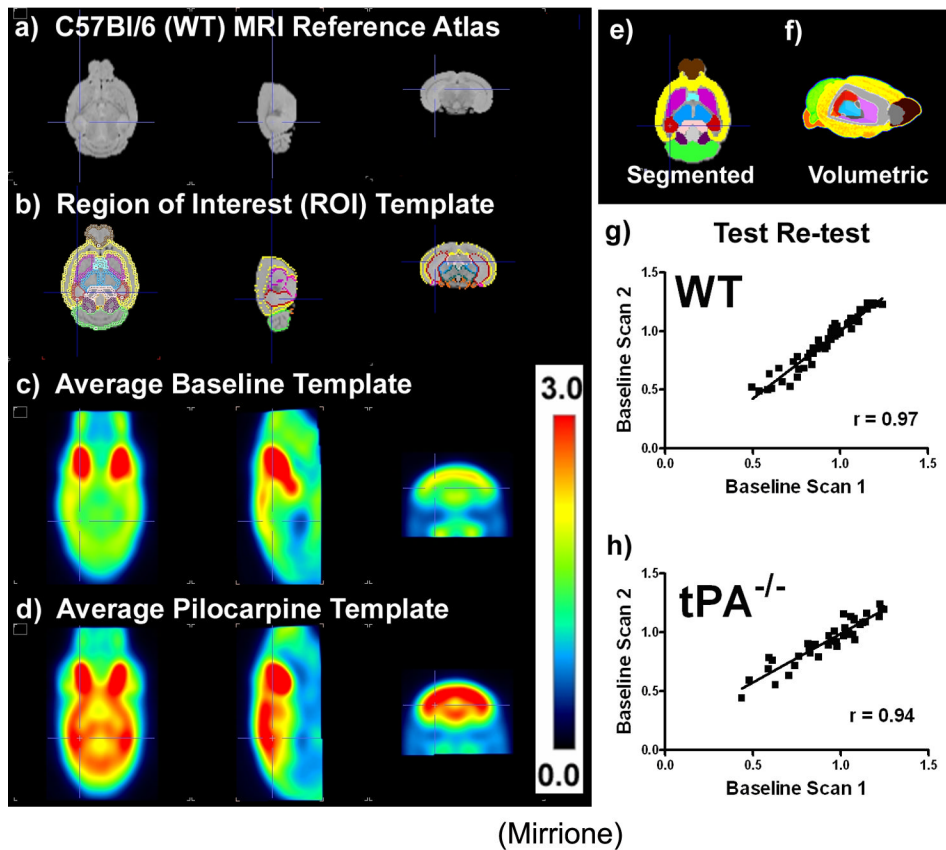
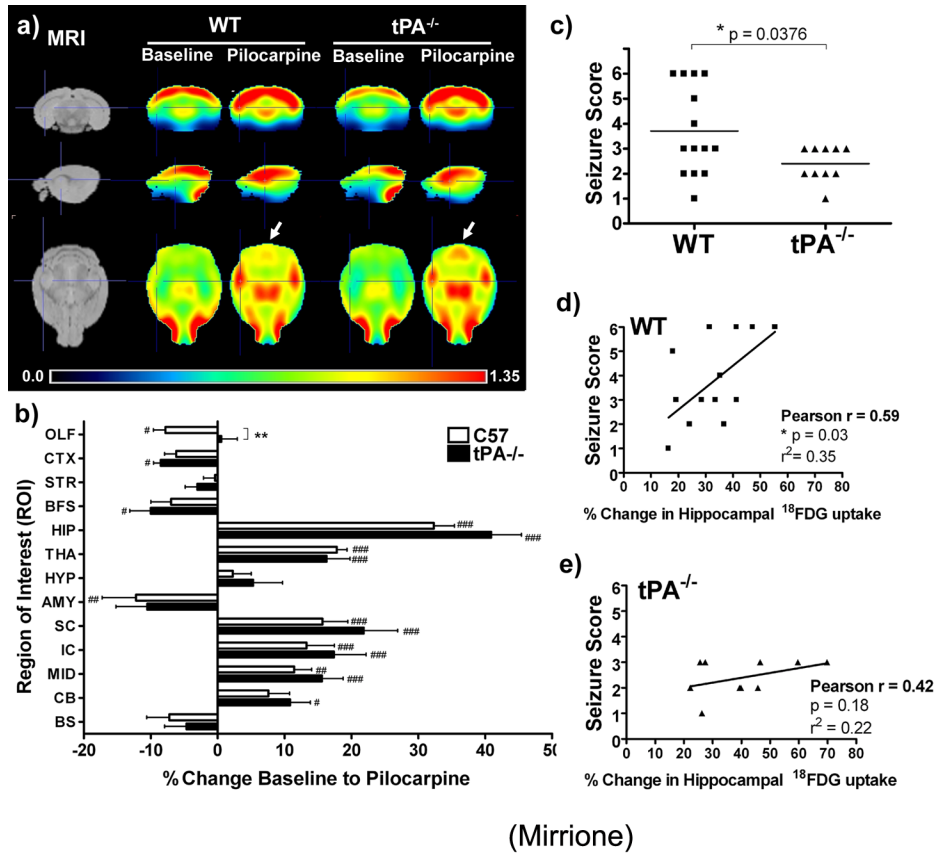


**Figure 1. Templates for mouse brain data analysis and validation of longitudinal design**  
 a) C57Bl/6J (wt) mouse MRI reference atlas (Ma et al., 2005) (left to right views, transverse, sagittal, coronal). b) Region of interest (ROI) template shown overlaid on the atlas, c) ROIs shown filled in and color coded on transverse plane, (brown = olfactory bulb, yellow = neocortex, red = hippocampus, purple = striatum, light blue = basal forebrain and septum, pink = amygdale, black = hypothalamus, light green = cerebellum, dark green = midbrain, dark purple = inferior colliculi, peach = superior colliculi, brain stem = orange). d) volumetric (3D) display of template regions with a cut out into the brain revealing the striatum in purple, thalamus in blue, and hippocampus in red, e)  $^{18}\text{F}$ FDG baseline template and f) pilocarpine treatment template. g) Ratio to whole brain ROI statistics calculated for each individual animal's baseline scan (scan 1) correlated with the second baseline scan (scan 2) one week later for wt (a,  $r^2=0.9427$ , slope= $1.154 \pm 0.04024$ ,  $p < 0.0001$ ,  $n=4$ ) and, h)  $t\text{PA}^{-/-}$  (b,  $r^2 = 0.8848$ , slope= $0.8312 \pm 0.04930$ ,  $p < 0.0001$ ,  $n=3$ ) shown to be significant by a Pearson coefficient & regression analysis with runs test for departure from linearity.

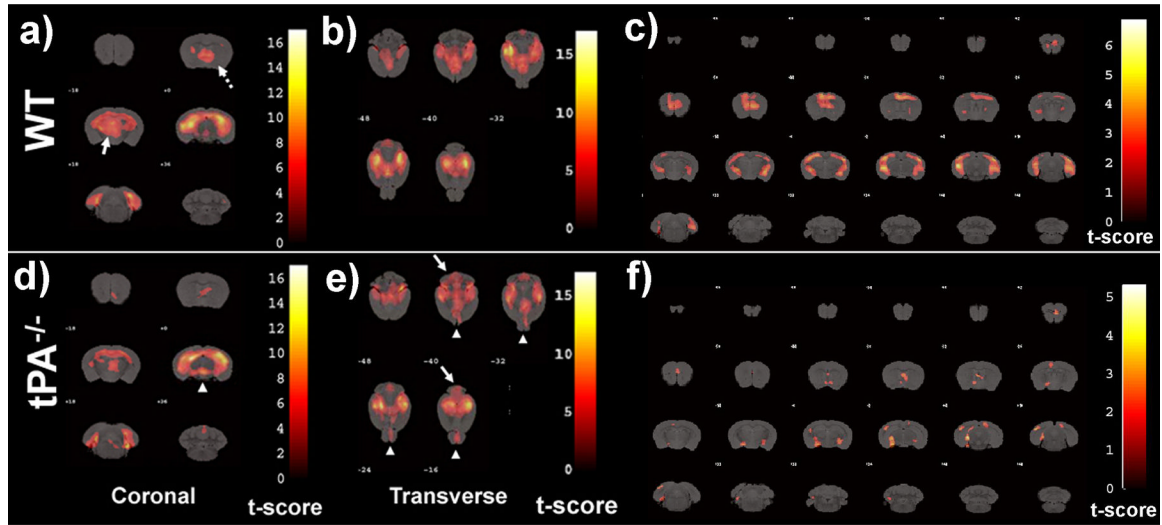


(Mirrione)

**Figure 2. Average regional <sup>18</sup>F DG uptake before and after acute seizures**

a) Individual spatially pre-processed images were skull stripped, globally normalized, and averaged together to create a representative brain radioactivity distribution map for each group (wt n=14, tPA<sup>-/-</sup> n=11) and shown in reference to the MRI template (top row: coronal, middle: sagittal, and bottom: transverse views). Relative ratio to whole brain intensity patterns are shown which demonstrate regional activations in the hippocampus and thalamus for both genotypes following pilocarpine administration and acute seizures. Arrows display an area of increased <sup>18</sup>F DG uptake in tPA<sup>-/-</sup> mice following seizures which was less apparent in the wt average image. Crosshairs are located at the hippocampus in all views. b) Percent change in <sup>18</sup>F DG uptake between baseline and seizure scan show significant increases in the hippocampus and thalamus for both genotypes, while tPA<sup>-/-</sup> mice show more significant activations in the midbrain and cerebellum when comparing baseline and post challenge scans. The percent change in <sup>18</sup>F DG uptake before and after seizures were significantly different between genotypes in the olfactory bulb. (Olfactory bulb (OLF), striatum (STR), basal forebrain and septum (BFS), cortex (CTX), hippocampus (HIP), thalamus (THA), hypothalamus (HYP), amygdale (AMY), cerebellum (CB), brain stem (BS), superior colliculi (SC), rest of mid brain (MID), and inferior colliculi (IC). (# = p<0.05, ## = p < 0.01, ### = p<0.001, two-way ANOVA with repeated measures and Bonferroni post-tests comparing baseline to pilocarpine average ROI values for each genotype, factor *treatment & ROI*; \*\* = p<0.01 Student's *t*-test comparing wt versus tPA<sup>-/-</sup> percent change for each region.). c) Behavioural analysis comparing seizure symptoms in wild type and tPA<sup>-/-</sup> mice show a significant difference in the distribution of seizure scores assigned to each animal based on symptoms during <sup>18</sup>F DG uptake (p=0.0376, two-tailed, unpaired *t*-test). d,e) Seizure scores correlated with percent change in hippocampal <sup>18</sup>F DG uptake baseline to post seizures. Note: in b, two points overlap (seizure score 2 and two animals showed a 24% change) and in c) two

points overlap (seizure score 2 and 39% change). Also note, behavioural data for one tPA<sup>-/-</sup> animal were accidentally not collected, and thus are not included in this analysis (wt n=14, tPA<sup>-/-</sup> n=10).



(Mirrione)

**Figure 3. Voxel based analysis for neuronal activation caused by seizures**

MRI reference template was overlaid with activations caused by seizures in wild type-mice (a-c) and tPA<sup>-/-</sup> mice (d-f). For wt mice, areas of increased activation compared to tPA<sup>-/-</sup> include septum (a, dotted arrow) and thalamus (a, arrow). For tPA<sup>-/-</sup> mice, areas of unexpected increased activation compared to wt mice include the midbrain (d, arrow head), cerebellum (e, arrows) and olfactory bulb (e, arrow heads). Thresholds for displayed images were set at P < 0.001 for coronal and P < 0.01 for transverse views in order to effectively reveal differences between genotypes. SPM covariate analysis to elucidate voxels where <sup>18</sup>FDG increased as a function of seizure severity in wt (c) and tPA<sup>-/-</sup> (f) mice. Voxels represent regions that increase in <sup>18</sup>FDG with seizure severity. The statistical threshold (t or p value) was set at p<0.05 with an extent threshold of 100 contiguous voxels. T-scores are represented by the color scale shown.

**Table 1**

Location <sup>†</sup> and volume of regions of interest in the ROI template

Brain Region	Abbreviation	Coordinates*			Volume <sup>‡</sup> mm <sup>3</sup>
		x	y	z	
Olfactory Bulb	OLF	±0.29	4.40	-2.34	22.44
Striatum	STR	±2.22	-0.05	-3.75	25.76
Basal forebrain & Septum	BFS	±0.29	0.68	-4.54	12.34
Cortex	CTX	±0.04	-1.18	-3.19	145.60
Hippocampus	HIP	±2.52	-3.14	-3.51	24.46
Thalamus	THA	±0.22	-2.14	-3.72	28.20
Hypothalamus	HYP	±0.25	-1.20	-5.54	11.56
Amygdala	AMY	±2.70	-1.67	-5.65	11.06
Cerebellum	CB	±0.25	-6.95	-3.80	57.19
Brain Stem	BS	±0.24	-6.46	-6.10	59.74
Superior Colliculi	SC	±0.16	-4.14	-2.35	8.71
Inferior Colliculi	IC	±0.86	-5.70	-2.40	7.38
Midbrain	MID	±0.44	-3.97	-4.38	17.90

<sup>†</sup> Locations determined in Paxinos & Franklin (2001) stereotaxic space and given as the center of each region relative to bregma (x: left to right, y: posterior to anterior, z: inferior to superior)

\* z-dimension is from the surface of the brain

<sup>‡</sup> both hemispheres

**Table 2**  
Brain Regions Correlated with Seizure Severity

<b>wt</b>	<b>Brain Region</b>	<b>Max <i>t</i></b>	<b>Avg <i>t</i></b>
Positive	Hippocampus	14.77	<b>6.44</b>
	Septum <sup>†</sup>	9.31	<b>1.33</b>
	Thalamus	13.30	<b>5.12</b>
	Midbrain	7.55	<b>0.79</b>
	Olfactory Bulb	0.00	<b>0.00</b>
	Cerebellum*	9.78	<b>0.31</b>
<b>tPA<sup>-/-</sup></b>	<b>Brain Region</b>	<b>Max <i>t</i></b>	<b>Avg <i>t</i></b>
Positive	Hippocampus	14.58	<b>5.91</b>
	Septum <sup>†</sup>	5.17	<b>0.19</b>
	Thalamus	14.71	<b>1.90</b>
	Midbrain	10.55	<b>2.66</b>
	Olfactory Bulb	6.18	<b>0.27</b>
	Cerebellum	12.97	<b>0.85</b>

Significant ( $p < 0.001$  corrected, or \*  $p < 0.002$  corrected) clusters resulting from a voxel-wise correlation between brain activity and seizure severity for wt and tPA<sup>-/-</sup> mice. Anatomical definitions of the clusters were made based on the mouse atlas (Paxinos & Franklin, 2001). Data presented include the maximum t-value within the region (same for all significance levels) and the average t value within the region (at  $p < 0.001$ ) presented as an average of the left and right hemisphere.

<sup>†</sup> Structure below the resolution of microPET.

**Table 3**

Measured parameters between groups

	Glucose (mmol/L)		Weight (gr)		Dose ( $\mu$ CI)		Uptake (min)	
	Mean	S.E.M.	Mean	S.E.M.	Mean	S.E.M.	Mean	S.E.M.
Wt baseline	19.42	$\pm 1.06$	27.81	$\pm 1.03$	558.60	$\pm 33.44$	59.36	$\pm 3.35$
Wt pilocarpine	17.46	$\pm 1.96$	27.48	$\pm 1.01$	594.10	$\pm 32.68$	63.36	$\pm 3.12$
tPA <sup>-/-</sup> baseline	14.25	$\pm 1.44$	27.67	$\pm 0.74$	560.40	$\pm 33.24$	64.36	$\pm 3.65$
tPA <sup>-/-</sup> pilocarpine	15.30	$\pm 1.92$	27.27	$\pm 0.69$	658.60	$\pm 50.45$	59.09	$\pm 2.26$

Glucose = whole blood measurements following the scan. Dose = amount of radiotracer injected. Uptake = time between radiotracer injection and start of scan.